Research

Multiple deletions of candidate effector genes lead to the breakdown of partial grapevine resistance to downy mildew

Manon Paineau[1,2] (iD), Andrea Minio[2] (iD), Pere Mestre[3] (iD), Frédéric Fabre[1] (iD), Isabelle D. Mazet[1] (iD), Carole Couture[1] (iD), Fabrice Legeai[4,5] (iD), Thomas Dumartinet[6] (iD), Dario Cantu[2,7] (iD) and François Delmotte[1] (iD)

[1]INRAE, Bordeaux Sciences Agro, SAVE, ISVV, F-33340, Villenave d'Ornon, France; [2]Department of Viticulture and Enology, University of California Davis, Davis 95616 CA, USA; [3]INRAE, Université de Strasbourg, SVQV, F-68125, Colmar, France; [4]INRAE, IGEPP, F-35650, Le-Rheu, France; [5]INRIA, IRISA, GenOuest Core Facility, F-35000, Rennes, France; [6]Univ. Bordeaux, INRAE, BIOGECO, F-33610, Cestas, France; [7]Genome Center, University of California Davis, Davis 95616 CA, USA

Authors for correspondence:
François Delmotte
Email: francois.delmotte@inrae.fr

Dario Cantu
Email: dacantu@ucdavis.edu

Summary

• Grapevine downy mildew, caused by the oomycete *Plasmopara viticola* (*P. viticola*, Berk. & M. A. Curtis; Berl. & De Toni), is a global threat to Eurasian wine grapes *Vitis vinifera*. Although resistant grapevine varieties are becoming more accessible, *P. viticola* populations are rapidly evolving to overcome these resistances. We aimed to uncover avirulence genes related to Rpv3.1-mediated grapevine resistance.

• We sequenced the genomes and characterized the development of 136 *P. viticola* strains on resistant and sensitive grapevine cultivars. A genome-wide association study was conducted to identify genomic variations associated with resistant-breaking phenotypes.

• We identified a genomic region associated with the breakdown of Rpv3.1 grapevine resistance (avrRpv3.1 locus). A diploid-aware reassembly of the *P. viticola* INRA-Pv221 genome revealed structural variations in this locus, including a 30 kbp deletion. Virulent *P. viticola* strains displayed multiple deletions on both haplotypes at the avrRpv3.1 locus. These deletions involve two paralog genes coding for proteins with 800–900 amino acids and signal peptides. These proteins exhibited a structure featuring LWY-fold structural modules, common among oomycete effectors. When transiently expressed, these proteins induced cell death in grapevines carrying Rpv3.1 resistance, confirming their avirulence nature.

• This discovery sheds light on the genetic mechanisms enabling *P. viticola* to adapt to grapevine resistance, laying a foundation for developing strategies to manage this destructive crop pathogen.

Introduction

Grapevine downy mildew, caused by the obligate biotrophic oomycete *Plasmopara viticola* (Berk. & M. A. Curtis; Berl. & De Toni), is one of the most destructive diseases world-wide (Viennot-Bourgin, 1949). The disease was endemic in North America (Rouxel *et al.*, 2013, 2014), where native grape species had developed genetic resistance, and it was accidentally introduced to southwest France in the 1870s from where it rapidly spread throughout Europe (Fontaine *et al.*, 2013, 2021). The Eurasian wine grape *Vitis vinifera* L. is highly susceptible to this disease, and disease control is mostly achieved through the use of fungicides. Grapevine breeding programs around the world have been producing new cultivars genetically resistant to the disease by introgressing known disease resistance *loci* from wild grape species. Most of the resistance to downy mildew found in grapevine is partial and caused by Resistance-genes (R-gene) that, depending on the resistance source, may explain up to 80% of downy mildew infection on the plant (Venuti

et al., 2013; Merdinoglu *et al.*, 2018). Over 30 downy mildew resistance *loci* have been identified in American and Asian *Vitis* species (Maul, 2021), but only few of them are currently being utilized in breeding programs: Rpv1 (Merdinoglu *et al.*, 2003), the two main haplotypes of the locus Rpv3 – Rpv3.1 and Rpv3.2 – (Welter *et al.*, 2007; Bellin *et al.*, 2009; Di Gaspero *et al.*, 2012), Rpv10 (Schwander *et al.*, 2012) and Rpv12 (Venuti *et al.*, 2013). Many of these cultivars are now commercially available and gaining popularity among growers, especially following the promotion of agroecological transition and pesticide use restrictions legislated by the European Union (European Commission, 2018).

Plasmopara viticola possesses a remarkable ability to evolve, as demonstrated by its rapid adaptation to synthetic fungicides (Chen *et al.*, 2007; Blum *et al.*, 2010; Delmas *et al.*, 2016). In addition to large population size and an obligatory sexual cycle (Gessler *et al.*, 2011), *P. viticola* boasts a highly repetitive genome, altogether granting it a great evolutionary potential (Dussert *et al.*, 2019, 2020). Consistent with this and despite a limited

deployment of disease-resistant grape cultivars in vineyards, resistance breakdowns have been reported (Peressotti *et al.*, 2010; Delmotte *et al.*, 2014; Delmas *et al.*, 2016; Gómez Zeledón *et al.*, 2017; Heyman *et al.*, 2021; Wingerter *et al.*, 2021; Paineau *et al.*, 2022), and some *P. viticola* strains are already capable of simultaneously overcoming several resistance loci at the same time, including Rpv3.1, Rpv3.2, Rpv10 and Rpv12 (Paineau *et al.*, 2022). The ability of *P. viticola* populations to rapidly adapt to resistant grapevines is concerning because of the substantial breeding efforts required to identify resistance sources and develop new resistant cultivars. Minimizing the risk of grapevine resistance gene depletion requires a better understanding on the genetic mechanisms responsible for pathogen adaptation to host resistance.

Grapevine resistance to downy mildew is marked by the triggering of hypersensitivity responses (HR), a rapid localized cell death around the point of infection aiming to stop the pathogen infection, upon infection by *P. viticola*, suggesting a gene-for-gene interaction between the plant and the pathogen (Bellin *et al.*, 2009; Paineau *et al.*, 2022). Most genetic factors of grape conferring resistance to downy mildew identified until now are located in genomic regions rich in nucleotide binding domain and leucine-rich repeat (NBS-LRR) genes (Di Gaspero *et al.*, 2007; Moroldo *et al.*, 2008; Merdinoglu *et al.*, 2018). The presence of NBS-LRR genes was confirmed by the cloning of the loci causing Rpv1 and Rpv3 resistance (Feechan *et al.*, 2013; Foria *et al.*, 2020). NBS-LRR proteins are involved in the recognition of specialized pathogen effectors. In oomycetes, the RXLR family is the largest and most studied family of cytoplasmic effectors. RXLR effectors are characterized by the presence of a signal peptide (SP), a RXLR-EER motif at their N-terminal sequence and one or more WY-domains, a common fold found only in this family of proteins (Anderson *et al.*, 2015). Structural studies revealed an additional fold present in many RXLR effectors, the LWY domain, which is often present in tandem repeats, conferring structural and functional modularity (He *et al.*, 2019). Related candidate effector proteins that possess a SP and carry WY-domains and the EER motif, but lack an RXLR motif, have been described in several downy mildews species (Derevnina *et al.*, 2015; Sharma *et al.*, 2015; Combier *et al.*, 2019; Wood *et al.*, 2020). To date, all the effectors of *P. viticola* that have been investigated were discovered through *in silico* predictions (Mestre *et al.*, 2016; Brilli *et al.*, 2018; Dussert *et al.*, 2019; Lan *et al.*, 2019; Lei *et al.*, 2019; Liu *et al.*, 2021; Ma *et al.*, 2021). While these studies have provided valuable insights into the mechanisms employed by the pathogen to infect its host, none of them have been reported to be directly related to a gene-for-gene interaction with resistance *loci*. Therefore, the specific effectors detected by grape resistance genes remain entirely unknown to date.

Rpv3.1 is the most exploited resistance in viticulture (Di Gaspero *et al.*, 2012). This resistance has been introduced from an unknown American grape species into the crop germplasm at the end of the 19th century. It is present in most of the French-American hybrids and in many modern varieties resistant to downy mildew. In response to *P. viticola* infection, Rpv3.1 activates effector-triggered immunity (ETI) and localized necrosis

(HR) in grapevine leaves (Bellin *et al.*, 2009). The causal factor for this resistance was recently mapped to a single locus of grapevine genome containing two TIR-NB-LRR (TNL) genes that originated from a tandem duplication (interleukin-1 receptor-nucleotide binding leucine-rich repeats (NLR)) (Foria *et al.*, 2020). On the pathogen side, rapid adaptation to Rpv3.1-mediated resistance has been reported in several geographically distant populations of *P. viticola* over the past decades (Peressotti *et al.*, 2010; Casagrande *et al.*, 2011; Delmotte *et al.*, 2014; Delmas *et al.*, 2016; Heyman *et al.*, 2021; Wingerter *et al.*, 2021; Marone Fassolo *et al.*, 2022; Paineau *et al.*, 2022). Overall, these findings suggest a gene-for-gene interaction between TNL genes of the plant and an undescribed avirulence gene of the pathogen.

In recent years, genome-wide association studies (GWAS) have become increasingly popular for identifying virulence/avirulence factors in fungal plant pathogens (Gao *et al.*, 2016; Zhong *et al.*, 2017; Hartmann *et al.*, 2018; Miller *et al.*, 2020; Phan *et al.*, 2021; Singh *et al.*, 2021; Kariyawasam *et al.*, 2022; Persoons *et al.*, 2022). In oomycetes, while the method has shown success in detecting the genomic regions underlying fungicide resistance and mating type (Siddique *et al.*, 2019; Dussert *et al.*, 2020), it has not yet been employed for discovering avirulence genes. In this study, we used GWAS to identify the avirulence genes interacting with Rpv3.1-mediated resistance of grapevine. To this end, we sequenced the whole genomes of 136 strains of *P. viticola* from a natural population in Bordeaux (France) and characterized their development on both resistant (Rpv3.1) and susceptible grapevines. By combining these data, we were able to identify candidate effectors and the genomic event responsible for the breakdown of Rpv3.1-mediated resistance.

Materials and Methods

Strains and plant materials

We collected 136 *Plasmopara viticola* (Berk. & M. A. Curtis; Berl. & De Toni) isolates in 2018 from two plots in Bordeaux vineyards located 5 km from one another (France). Further details about their origin are provided in the Data Availability section (doi: 10.57745/U6JECD). The monosporangium isolation was carried out as described in Paineau *et al.* (2022). After monosporangium isolation, isolates are referred as 'strains'. After 2 wk of propagation (Supporting Information Methods S1), on the day of inoculation, the strains were suspended in sterile water and the density of the suspension was adjusted to 5×10^3 sporangia ml^{-1} in a volume of 120 ml. Two host plants were used for the phenotyping experiment. *Vitis vinifera* cv. Cabernet sauvignon (CS; Rpv3.1-) was chosen as a susceptible host to downy mildew and the variety 'Regent' as a partially resistant host carrying the resistance Rpv3.1 (Rpv3.1+). The plants, 75 of each variety, were grafted onto the Selection Oppenheim 4 (SO4) rootstock and grown simultaneously in a glasshouse under natural photoperiod conditions 12 h : 12 h, day : night on average, without chemical treatment. The inoculation and phenotyping experiment was conducted on the fourth leaf below the

apex (one leaf per plant), which was collected after 6 months of cultivation.

Phenotyping experiment

We inoculated the 136 strains on the susceptible variety *V. vinifera* cv. CS and the resistant variety 'Regent'. Four mock strains consisting of sterile water were used as negative controls. For each of the 280 interactions, we performed six replicates. We therefore generated 1680 plant–pathogen interactions in total (i.e. grapevine leaf disk inoculated with a *P. viticola* strain) as described in Methods S2. The leaf disks were placed in 36 square Petri dishes (23 × 23 cm), with each of the six replicates placed in a different Petri dish. Petri dishes were sealed with Parafilm to maintain relative humidity at 100%. They were then incubated in three growth chambers, paying attention to have the six replicates equally represented in the three different growth chamber, for 6 d at 23°C under a 12 h : 12 h, light : dark photoperiod. Six days post-inoculation, all leaf disks were photographed and the sporulation area per disk was determined by image analysis (code available at https://github.com/ManonPaineau/image_analysis_P.viticola) as described in Paineau *et al.* (2022).

Genotyping

The DNA from the 136 strains was extracted directly from the mycelium of *P. viticola* with a DNA extraction protocol adapted from Möller *et al.* (1992; Methods S3). Sequencing was performed at the GeT-PlaGe facility (Toulouse, France) with a NovaSeq6000 and a Hiseq4000 (2 × 150 bp paired-end reads) (Methods S4). The variant calling was performed using GATK (McKenna *et al.*, 2010) as described in Methods S5. After a quality control (Methods S6), we kept a final dataset consisting of 123 strains for the GWAS panel encompassing a total of 1 851 765 polymorphic nucleotides. Finally, population genetic structure was investigated by principal component analysis (Methods S7).

Genome-wide association study

The GWAS was performed on the sporulation area quantitative trait using the exact Genome-wide Efficient Mixed Model Association (GEMMA) method (Zhou & Stephens, 2012). The association tests were realized with the relatedness matrix, estimated with the GEMMA software (http://www.xzlab.org/software.html), phenotype (average sporulation area value on Regent (Rpv3.1+) for the six replicates) and genotype (filtered single nucleotide polymorphisms (SNPs)). GEMMA also estimated the proportion of phenotypic variation explained (PVE) by genotypes. We corrected the significance threshold by the Bonferonni criterion calculated as $-\log_{10}(\alpha/k)$, where k is the number of statistical tests conducted and $\alpha = 0.05$. We verified that the model fits our data and correctly accounted for population structure by checking the quantile–quantile plot and the degree of deviation of the genomic inflation factor lambda (λ) defined as the median of the resulting chi-squared test statistics divided by the expected median of the chi-squared distribution. The quantile–quantile plots and Manhattan plots were visualized with the R package QQMAN (Turner, 2018). We analyzed the linkage disequilibrium of the SNPs around the identified loci using the package LDHEATMAP implemented in R (Shin *et al.*, 2006).

Genome reassembly and avrRpv3.1 locus analysis

Whole genome assembly of Single Molecule Real-Time (SMRT) reads (Dussert *et al.*, 2019) was performed in a two-step procedure using the customized FALCON-Unzip pipeline as reported in Minio *et al.* (2019; https://github.com/andreaminio/FalconUnzip-DClab). The details of the assembly procedure are described in Methods S8. We compared the two INRA-Pv221 assemblies to identify, in the new diploid assembly, the location of the loci identified by GWAS in the consensus reference genome. We used NUCmer with the minimum cluster size $c = 65$ and visualize the result with mummerplot from the MUMMER3 software (Kurtz *et al.*, 2004). To evaluate the copy number variation (CNV) in the locus, the short reads of each sample were aligned separately with BWA MEM (v.0.7.17, Li, 2013) on *P. viticola* strain INRA-Pv221 FalconUnzip primary assembly, and copy number was evaluated on the entire dataset with CNVKIT (v. CNVKIT 0.9.9, Talevich *et al.*, 2016). To visualize the allelic count, per-base mapping coverage was calculated with SAMTOOLS depth (v.1.10, Li *et al.*, 2009), and mean coverage value was calculated on windows of 1 kbp in size and normalized on the sample diploid whole genome mean coverage. Additional analyses of the avrRpv3.1 locus, including phylogenetic analyses, population genetic analysis and analysis of the locus for two independent European strains, are detailed in Methods S9–S11, respectively.

Gene expression analysis

To find evidence of expression for the genes present in the avrRpv3.1 locus during the host–pathogen interaction, we aligned the available raw RNA-seq data from Dussert *et al.* (2019) (SRR accession list available in doi: 10.57745/U6JECD) on the avrRpv3.1 locus. The trimming, alignment and expression analysis of the transcripts were performed as described in Methods S12. In order to differentiate reads from *P. viticola* and *V. vinifera*, the paired-end reads were aligned against both haplotypes of INRA-Pv221, newly assembled with Falcon Unzip in this study, and the first haplotype of *V. viniferae* cv Cabernet sauvignon genome v.1.1 (Massonnet *et al.*, 2020).

Predicted protein analysis

BLASTP searches were performed against the NCBI nr protein database. Signal peptides were predicted with SIGNALP v.6.0 (Teufel *et al.*, 2022). Structural similarity searches were performed on Phyre2 (Kelley *et al.*, 2015) and HHPred (Gouy *et al.*, 2010), and displayed with Boxshade. Structural prediction of g166 structure was performed using ALPHAFOLD2 (Jumper *et al.*, 2021) implemented at COLABFOLD (Mirdita *et al.*, 2022) using default settings. Visualization and superimposition of

predicted structures was performed on UCSF Chimera X 1.5 (Goddard *et al.*, 2018). The predicted structure of the *Plasmopara halstedii* and *Phytophthora sojae* PSR2 proteins were retrieved from the EBI ALPHAFOLD2 database (https://alphafold.ebi.ac.uk/entry/A0A0P1AQR5) and (https://alphafold.ebi.ac.uk/entry/E0W4V5), respectively.

Semi-quantitative reverse transcription polymerase chain reaction

RNA extraction, cDNA synthesis and PCR were done as in Mestre *et al.* (2017). Each sample from infected tissues consisted of four leaf disks. Briefly, after RNA extraction, DNAse treatment was done using the Invitrogen-Turbo DNA free kit, and first-strand cDNA was synthetized using the RevertAid First Strand cDNA synthesis kit (Thermo Scientific, Waltham, MA, USA). PCR amplifications consisted of 30 cycles of 20 s at 94°C, 20 s at 58°C and 60 s at 72°C, followed by a final extension step of 10 min at 72°C. Primers are listed in doi: 10.57745/U6JECD.

Transient assay

The coding sequences of g164, g165 and g166 without the predicted SP were PCR-amplified with Phusion polymerase (NEB) from genomic DNA of *P. viticola* strain INRA-Pv221. Following amplification with primers containing restriction sites, the PCR products were digested (NEB restriction enzymes) and cloned directionally into plasmid pBIN61. Plasmids were transformed into *Escherichia coli* strain DH10B by electroporation. Qiagen Plasmid Mini Kit was used to extract the plasmids from the *E. coli* cultures, and Agrobacterium strain C58C1 carrying the pCH32 plasmid was then transformed by electroporation. The identity of the clones was confirmed by sequencing. Primers used for cloning are listed at doi: 10.57745/U6JECD. Agrobacterium cultures were grown at 28°C in 5 ml of L medium containing kanamycin (50 µg ml^{-1}) and tetracycline (2.5 µg ml^{-1}). After 2 d, 1 ml of the bacterial suspension was used to inoculate 5 ml of L medium containing kanamycin (50 µg ml^{-1}), tetracycline (2.5 µg ml^{-1}), 10 mM MES and 150 µM acetosyringone, and grown in the same conditions for 1 d. Bacterial suspensions were centrifuged, and the pellets were resuspended in a solution containing 10 mM MES, 10 mM MgCl2 and 150 µM acetosyringone. After 2–3 h of incubation at room temperature, bacterial suspensions were infiltrated at an optical density at 600 nm (OD600) of 0.4 using a needleless syringe. Infiltrations were performed, as detailed in Methods S13, on detached leaves collected from green cuttings of Regent (Rpv3.1+) and the susceptible *V. vinifera* cultivar Syrah (Rpv3.1−).

Results

Localization of the virulence locus by GWAS

To identify the avirulence genes interacting with Rpv3.1-mediated resistance of grapevine, we performed a GWAS on a *Plasmopara viticola* population composed of 136 strains sampled on both sensitive (Rpv3.1−) and resistant (Rpv3.1+) cultivars. The sequences of 123 strains passed quality control (Methods S6). A total of 1851 765 SNPs were retained, resulting in an average density of 20.8 SNPs/kbp on the 359 scaffolds of the *P. viticola* reference genome INRA-Pv221. To assess the phenotypic variability of the 123 *P. viticola* strains, we evaluated the percentage of leaf disk area covered by sporulation in a cross-inoculation experiment between the 123 *P. viticola* strains and two grapevine varieties: CS (susceptible, Rpv3.1−) and Regent (Rpv3.1+) (Fig. 1b). On CS, the strains displayed an average of sporulation of 10.4% (SD = 3.04) (Fig. 1b). On Regent, the average sporulation area of the strains was 7.22% (SD = 6.63) (Fig. 1b). Levels of sporulation on Regent and CS did not correlate (Fig. S1). While the distribution of sporulation area of the strains on CS is centered around the mean, the sporulation variability among strains observed on Regent ranged from 0.01% to 29.33% and follows a bimodal distribution (Fig. 1a): The larger group, comprising the majority of observations, is concentrated in the first quartile (Q1), with a 25th percentile value of 1.12% of sporulation area. Conversely, the second group is predominantly situated in the third quartile (Q3), as evidenced by the 75th percentile value of 11.79%. The bimodal distribution underscores the presence of two discernible subpopulations with contrasting levels of sporulation on Regent.

We used the sporulation area of the strains on Regent as a quantitative trait to perform a GWAS. We used a GEMMA to correct for the population structure bias evidenced by the principal component analysis (Fig. S3). The quantile–quantile (Q-Q) plot showed no evidence of inflation in test statistics for the sporulation on Regent (λ = 1.04) (Fig. S4). Finally, the proportion of PVE estimated by GEMMA was 0.58, indicating that genetic variants account for 58% of the phenotypic variance in our population. Despite the significant contribution of genetic data to explaining variance, it is crucial to recognize that environmental conditions (e.g. temperature and plant physiological status) also influence the quantitative interaction between grapevine and downy mildew.

We identified a total of 74 markers strongly associated with this phenotypic trait (Fig. 1c). On the scaffold Plvit038, the 66 markers are located in an interval of 3340 bp (Figs 1D, S5A,B) and exhibit strong linkage disequilibrium (Fig. S5D). No gene nor pseudogene was detected at this location on the genome assembly (Figs 1d, S5C). In the locus on scaffold Plvit053, eight markers, in an interval of 144 bp, were significantly associated with the sporulation on Regent (Figs 1d, S5A,B) and are in strong linkage disequilibrium (Fig. S5D). The significant SNPs identified by GWAS are at the edges of Plvit038 and Plvit053 scaffolds (Fig. S5A) and show evidence of being tightly associated as observed by a strong linkage disequilibrium (Fig. 1d). The high R^2 values *c.* 0.7 observed between the two scaffolds indicate a close physical proximity of the sequences, which appears to have been disrupted by the fragmentation of the genome assembly. Based on the gene annotation (Dussert *et al.*, 2019), one gene is located in this region: PVIT-0015215.T1 (Fig. 1d).

A structural rearrangement identified in the avrRpv3.1 locus

To investigate the relationship between the two loci identified by GWAS and to identify potential differences between haplotypes, we employed Falcon Unzip to build *de novo* a phased diploid *de novo* genome assembly using as input the same SMRT reads that were assembled in the haploid consensus genome used as reference for GWAS (Chin *et al.*, 2016). We reconstructed and annotated both alternative haplotypes of INRA-Pv221 (Table S1). The primary assembly, which represents the most contiguous haploid representation of the genome, comprised 80.6 Mbp, divided into 252 primary contigs, and contained 23 602 protein coding gene loci. The genome size of this new assembly (80.6 Mb) is comparable to previous assembly results but falls intermediate between a previous SMRT sequencing assembly (92.94 Mb, Dussert *et al.*, 2019) and an Illumina assembly (74.74 Mb, Dussert *et al.*, 2016). This is attributed to the combined effect of improved representation of repetitive content enabled by long reads and the utilization of a diploid-aware procedure capable of effectively segregating highly divergent alleles into haplotigs (i.e. phased alternative haplotypes). Moreover, with the longest sequence reaching 3.17 Mbp and an N50 of 825.8 kbp (N50 index 29), the new diploid assembly exhibits enhanced sequence contiguity compared with previous *P. viticola* strain INRA-Pv221 assemblies (Dussert *et al.*, 2016, 2019). Falcon-Unzip reported a separate alternative haplotype representation for over 66.5% of the *P. viticola* genome (53.6 Mb in 745 Haplotigs, 15 642 protein coding gene loci), confirming the extensive structural variability present between haplotypes in the INRA-Pv221 strain.

By aligning the scaffolds Plvit038 and Plvit058 with the sequences of both primary contigs and haplotigs of the diploid reference, we confirmed the contiguity of the two scaffolds within the same genomic region (Fig. S6A,B). This was ascertained by their juxtaposition on both a primary contig (Primary_000014F) and one of its associated haplotigs (Haplotig_000014F004), as illustrated in Fig. S6(C,D). Additionally, we discovered the presence of structural variations between the two haplotypes within this locus, hereafter named avrRpv3.1. These structural variations were identified in the vicinity of the anticipated gene locus that encodes PVIT_0015215.T1. A structural variation event involving a 30 kbp deletion was observed (Figs 2, S7) at this locus. Specifically, the genomic region spanning from 695 to 725 kbp in Primary_000014F is absent from Haplotig_000014F004. This finding suggests that the consensus haploid assembly (Dussert *et al.*, 2019) exclusively represented the structure of the locus represented in the haplotig sequences. The deletion and the other structural variants found in the locus affect three coding gene loci: Primary_000014F.g163, Primary_000014F.g164 and Primary_000014F.g165 (hereafter called g163, g164 and g165). The gene g163 is translocated along with a transposable element (TE) found in this region (Fig. 2). We discarded g163 from the following analyses as it is not deleted and is related to TEs. The genes g164 and g165, which were absent in the consensus assembly, are deleted in the haplotig and were not found to be duplicated in the genome. Gene PVIT_0015215.T1 of the consensus assembly corresponds to gene g166 from the diploid assembly (99.9% coverage and 98% identity), located right next to the deletion and present in both haplotypes (Fig. 2). The genes g164 and g165 are called hereafter avrRpv3.1 genes.

To gain a comprehensive understanding of the distribution of avrRpv3.1-like genes in *P. viticola* and other oomycete plant pathogens, we utilized the sequence of g164 as a query and conducted a search through oomycete genomes available in GenBank using BlastP. A total of 11 sequence matches were found in *P. viticola* genome, including g164 and g165, and 14 sequences in the genome of *P. halstedii*, one of which being annotated as an RXLR-like protein. No sequence matches were observed outside the genus *Plasmopara*, including *Bremia*, *Phytophthora* and *Pythium* species. Interestingly, the 11 sequences of *P. viticola* were organized in a single cluster within the contig Primary_000014F (Fig. S8). Within *P. viticola*, the gene size ranged from 2535 to 2688 bp with a mean size at 2650 bp. The 11 *P. viticola* proteins presented a high degree of similarity estimated by pairwise comparison of sequences (average of 61% identity). The phylogenetic analyses (Fig. S8) indicated that g162, g164, g165, g166 and g169 formed a well-supported group among which g164 and g165, the two genes included in the deletion, were the closest relatives (69.76% of conserved amino acids). The nine genes are now considered as avrRpv3.1-like genes. Altogether, the analyses of avrRpv3.1 candidate genes evidenced that a genus-specific gene family expansion has occurred through tandem duplication events in the *P. viticola* genome.

Allelic diversity at the avrRpv3.1 locus

We then assessed whether the absence of avrRpv3.1 genes correlates with the strains' phenotype, specifically their virulence on Rpv3.1+ grapevine cultivars. The identification of a 30 kpb deletion within one of the two haplotypes in the INRA-Pv221 strain suggests the likely presence of a minimum of two alleles at this locus. To comprehensively investigate the variability of this locus within *P. viticola* and its potential correlation with strain virulence, we analyzed the association between virulence and the allelic variation at the avrRpv3.1 locus (interval between 640 and 740 kbp of Primary_000014F) across the 123 *P. viticola* strains.

For each strain, we performed a diploid-aware CNV analysis to identify regions with significant difference in sequencing coverage compared with the rest of the contig (Primary_000014F) and detect the underlying structural variants (Figs 3a, S9, S10). We observed that the deletion at the locus avrRpv3.1 is variable in size, evidencing the existence of multiple allelic forms. We identified the presence of one allele without any deletion (Avr) and six alleles (avr1-6) presenting deletions ranging from 14 to 96 kbp (Fig. S11). The high density of TEs in this region impacts the accuracy of the deletion coordinates. The deletion impacted the presence of genes g164 and g165. The five avr alleles share a deletion of the gene g164, which is complete in all alleles, except for avr2 where g164 is only partially deleted. The gene g165 is present in avr3, partly deleted in avr2 and avr4, and fully deleted in avr1, avr5 and avr6 (Figs 3b, S11).

Through CNV analysis, nine distinct allelic configurations were identified among the 123 strains (Fig. 3b): 59 were homozygous for the Avr allele, 12 were heterozygous (Avr/avr) and 52 displayed a deletion on both haplotypes (avr/avr). The Avr allele was thus the most frequent one (53%) followed by avr1 (39%). The frequency of the five other avr alleles represented 8% of the population and varied from 0.5% to 3%. The average sporulation area associated with each genotype on both CS (Rpv3.1−)
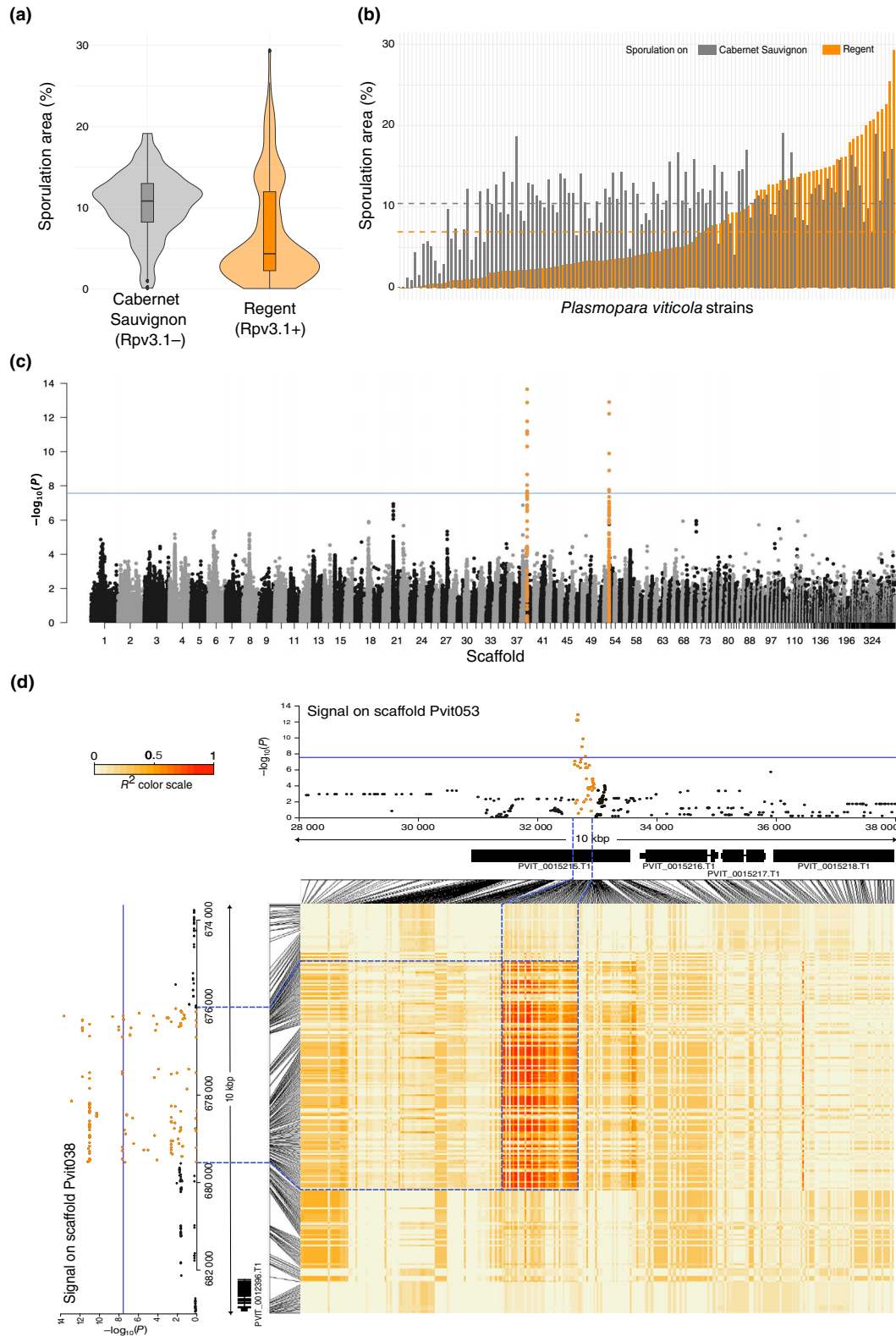
Fig. 1 Result of association genomics analysis of *Plasmopara viticola* virulence on the resistant variety Regent carrying Rpv3.1. (a) Violin plots showing the distribution of the sporulation area of the population on Cabernet sauvignon (CS; Rpv3.1⁻, gray) and Regent (Rpv3.1⁺, orange). Boxplots's horizontal lines correspond to the 25th, 50th and 75th percentiles, vertical lines extend between the smallest and largest value no further than 1.5 × interquartile range. (b) Histogram of the sporulation area of each of the 123 strains on CS (gray) and Regent (orange). Values correspond to the mean of sporulation area in percentage for six replicates. The horizontal dashed lines represent the average of the population on CS (gray) and Regent (orange). The SE and strain names are not depicted for readability of the figure and are deemed unnecessary for comprehension, but they are provided in Supporting Information Fig. S2 and via doi: 10.57745/U6JECD. (c) Manhattan plot of the whole genome highlighting two significant loci linked to Rpv3.1 virulence. Each point represents a single single nucleotide polymorphisms (SNP). The *x*-axis shows SNP positions across scaffolds, while the *y*-axis indicates significance in relation to Rpv3.1 virulence. The blue line denotes the Bonferroni-corrected significance threshold (alpha = 0.05); SNPs below this line are not significant. *Loci* associated with Rpv3.1 virulence are marked in orange. The first signal is located on scaffold Pvit038 and the second on Pvit053. (d) The heatmap illustrates the Linkage Disequilibrium (R^2) between the two signals identified by genome-wide association studies. Two Manhattan plots provide an enlarged view, spanning 10 Kpb, of the specific loci situated on scaffolds Plvit038 (*y*-axis) and Pvit053 (*x*-axis), as depicted in (c). The heatmap showcases the R^2 values between each SNP from scaffold Pvit038 and those from scaffold Pvit053, as presented on the Manhattan plots above. The genes' positions within the loci are indicated beneath the Manhattan plots. The connection between SNPs in the Manhattan plots, their positions within genes and their corresponding R^2 values in the matrix is denoted by the black lines flanking the matrix. Notably, the two loci significantly associated with virulence on Rpv3.1, displayed in (c) demonstrate a high level of linkage disequilibrium ($R^2 > 0.7$) and are highlighted with blue dashed lines.
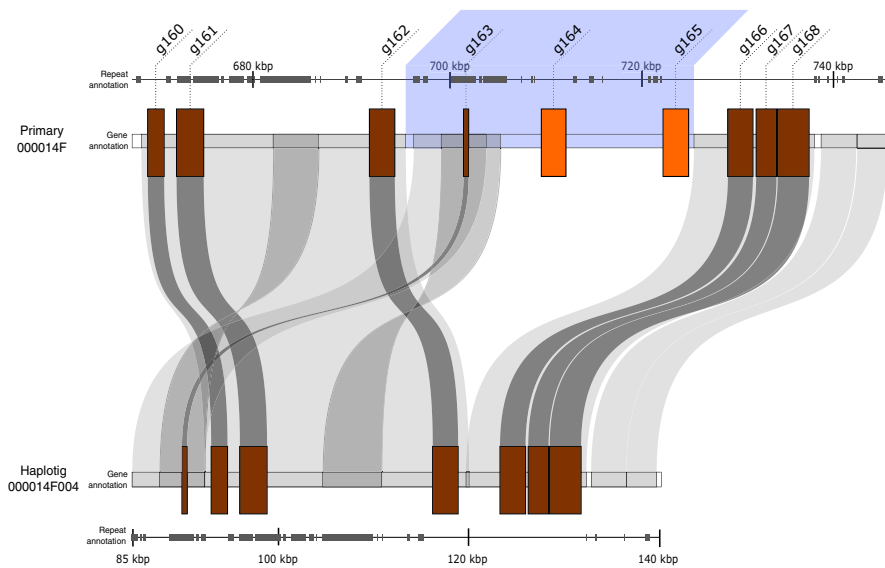

Fig. 2 Structural representation of the locus avrRpv3.1, associated with virulence against Rpv3.1 resistant grapevine. Both haplotypes, Primary_000014F (top) and Haplotig_000014F004 (bottom) of the newly assembled reference genome INRA-Pv221, are represented. The genes annotation is shown as brown squares. The two genes deleted from the haplotig, g164 and g165, are highlighted in orange. The repeat annotation is represented in gray on the scale of both haplotypes. The deletion associated with this locus, identified through genome-wide association studies, is highlighted in blue. The links between the Primary and Haplotig sequences (as well as between genes) connect regions showing significant homology, indicating that the sequences from the Primary are similar to those on the underlying Haplotig (Supporting Information Fig. S7).

and Regent (Rpv3.1+) is depicted in Fig. 3(c,d). Strains with the Avr/Avr genotype, that is homozygous without any deletion, display four times more sporulation area on CS (mean = 9.31%) than on Regent (mean = 2.4%). The avr/avr genotypes have a similar or higher sporulation on Regent (mean = 12.91%) than on CS (mean = 11.42%). Finally, the Avr/avr genotypes display a sporulation two times more important on CS (mean = 11.62%) than on Regent (mean = 6.41%) (Fig. 3d). It may be noted that strains Avr/avr have a sporulation level on Regent that is variable, ranging from 5% to 15% of the sporulation area (Fig. S12). Overall, we concluded that the breakdown of the Rpv3.1 resistance results from the structural variations at the locus avrRpv3.1.

Additionally, we examined the avrRpv3.1 locus in two another *P. viticola* strains collected from Switzerland that exhibited virulence on Rpv3.1-resistant varieties (strain 'avrRpv3-Rpv12-' in Wingerter *et al.*, 2021) and 'Pv412_11' in Paineau *et al.* (2022). Using the same pipeline analysis as for our *P. viticola* population, we observed, for the strain 'avrRpv3-Rpv12-', a 30 kbp deletion in one haplotype and a 56 kpb deletion in the other at this locus (Fig. S13). This matched the avr1/avr5 allelic configuration of *P. viticola* identified in our population. For the strain 'Pv412_11', we observed a 14 kpb deletion corresponding to the allele avr2 and a 78 kbp deletion (from *c.* 648 to 726 kpb) (Fig. S14) that does not correspond to any of the alleles described in this study but is similar to avr5 and avr6. This deletion also

impacts both genes g164 and g165. Overall, the results obtained on *P. viticola* strains from a different geographical origin confirm that structural variations at the avrRpv3.1 locus are involved in the breakdown of Rpv3.1 resistance.

Based on the allelic configurations described above, the avrRpv3.1 locus revealed to be in strong Hardy–Weinberg (HW) disequilibrium (*P*-value = 1.34e-21) with a negative *D* value (*D* = −24.65), suggesting a strong deficit of heterozygous genotypes. This result contrasts with results obtained along the contig Primary_000014F, where more than 95% of the SNPs were at HW equilibrium as expected for neutral markers in panmictic populations. We also observed a high genetic differentiation
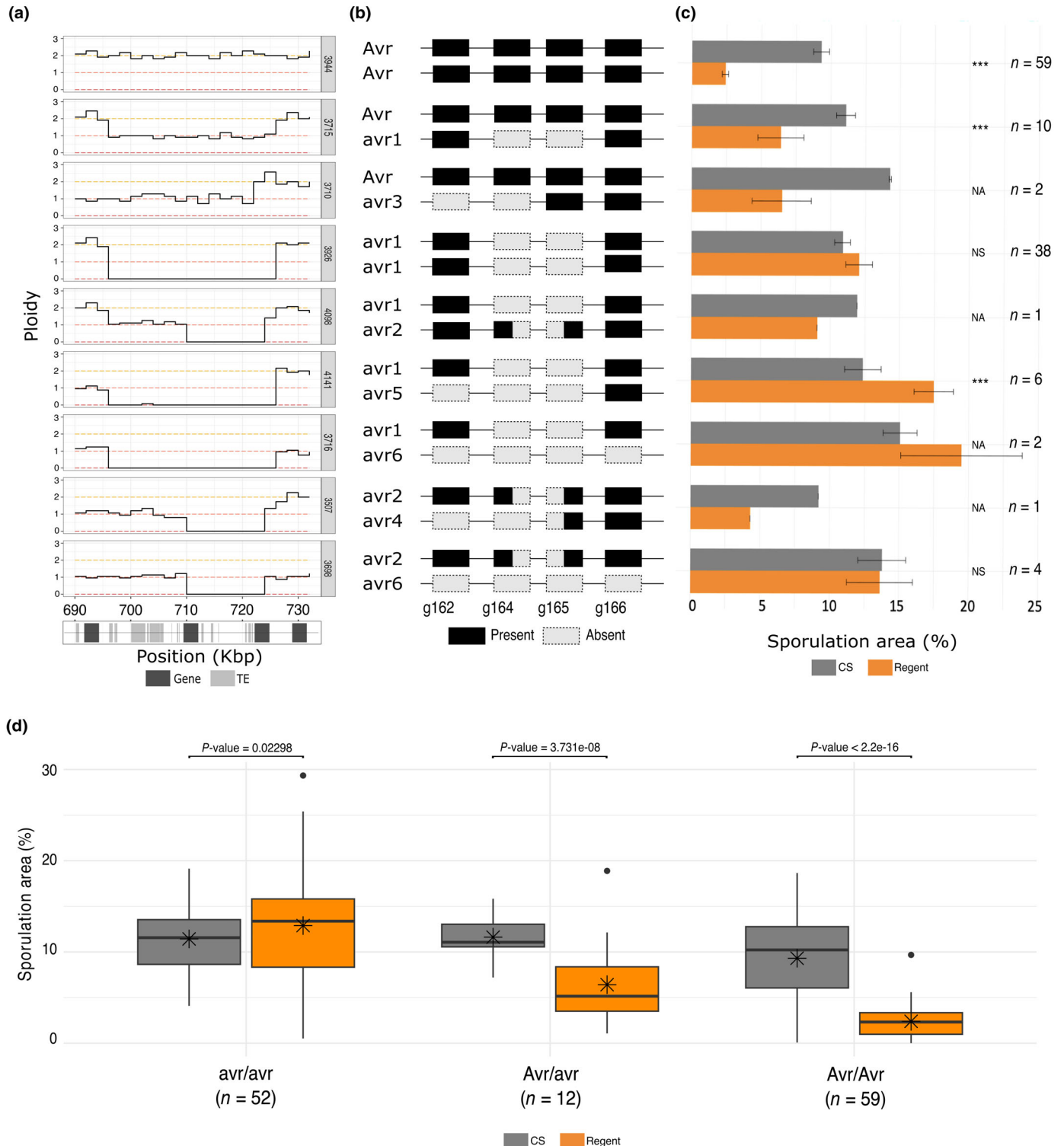
Fig. 3 Allelic configuration analysis of the 123 *Plasmopara viticola* strains at the locus avrRpv3.1. (a) Coverage patterns in the avrRpv3.1 locus. The coverage is represented in a sliding window of 2 kbp, illustrating the presence or absence of sequences in both haplotypes (ploidy of two), in one haplotype (ploidy of one), or a complete deletion in both haplotypes (ploidy of 0). Each allelic configuration is represented by a single strain. Details for the entire locus, from 640 to 740 kbp, for the 123 strains, are provided in Supporting Information Figs S9 and S10. The coverage plots are represented the location of transposable elements (light gray) and genes (dark gray) for this region. (b) Schematic representation of the diploid locus with gene presence/absence. Genes correspond to the genes presented in (a). Black rectangles denote gene presence, dashed gray rectangles indicate gene deletion, and black with dashed gray rectangles indicate partial gene deletion. (c) Phenotypic variation in sporulation area on Cabernet sauvignon (CS) (gray) and Regent (orange) for each allelic configuration. (***) indicates a significant difference (*P*-value < 0.01) between CS and Regent, 'ns' denotes no significant difference, and 'na' signifies tests not performed due to insufficient replicates. Error bars indicate SE. '*n*' indicates the number of strains for each category. (d) Boxplots summarize the phenotypic variation from (c), representing homozygous Avr/Avr genotypes without any deletion, Avr/avr genotypes with the deletion of one of the haplotypes, and avr/avr genotypes with a deletion on both haplotypes. Boxplots's horizontal lines correspond to the 25th, 50th and 75th percentiles, vertical lines extend between the smallest and largest value no further than 1.5 × interquartile range. Black stars correspond to the mean. The *P*-value indicated is the results of a nonparametric Kruskall–Wallis test. '*n*' indicates the number of strains for each category.

(F_{ST} = 0.58) between strains sampled on the susceptible and the resistant varieties at the locus while the average F_{ST} calculated across the contig was found to be 0.03 ± 0.05 with 99% of the F_{ST} values lower than the value calculated at the avrRpv3.1 locus (Fig. S15). The heterozygote deficits and strong genetic differentiation between strains collected on susceptible and resistant grapevines may result from host selection occurring at the avrRpv3.1 locus.

The candidate genes of the avrRpv3.1 locus encode putative effector proteins

We have established the correlation between the breakdown of Rpv3.1 and the deletion of genes within the avrRpv3.1 locus. This led us to explore in more detail the functionality and characteristics of these deleted genes. The genes g164, g165 and the related gene g166 encode proteins of 800–900 amino acids with a putative SP and without detectable conserved domains. All proteins contain an EER motif and repeat motifs (Fig. S16). Although they did not contain RXLR or RXLR-like motifs in their N-terminal region, structural similarity searches using HHPred and Phyre2 produced best hits with the structures of RXLRs effectors PSR2 from *Phytophthora sojae* and PcRXLR12 from *Phytophthora capsici*.

The structural similarity to oomycete effectors prompted us to pursue structural analyses. Indeed, because the LWY fold is only found in oomycete effectors, finding it in our candidate proteins would support their potential role as effector proteins. We modeled the structure of g164, g165 and g166 using AlphaFold2. Because the backbone structures of g164, g165 and g166 are very similar (Fig. S17), we describe the results of further structural analyses focusing on g164. The overall quality parameters of the model allowed to be confident in the backbone structure (Fig. S18A,B). The g164 predicted structure is horseshoe-shaped and similar to the Alphafold-predicted structure of a related protein from *P. halstedii* (Fig. S18C,D). Because the predicted structure appeared modular, we hypothesized that it was composed of repeats of the LWY-fold. We divided the g164 predicted structure into structural modules based on the *P. sojae* RXLR effectors PSR2 LWY domain structure, starting at the N terminus with the alpha-helices corresponding to the helix bundle 1 (HB1) of the LWY domain. The g164 structural modules obtained, which

we tentatively named LWY modules, produced a good overlap between them at the N terminus but they were different at the C terminus (Fig. S19A). Furthermore, the superimposition of the PSR2 LWY motifs and the g164 LWY modules revealed an overlap at the level of the PSR2 LWY HB1 but a different structural organization for HB2 (Fig. S19B).

We divided the g164 predicted structure into modules that contained the HB1-like sequence at the C-terminal part, resulting in a protein consisting of nine modular repeats, most containing five alpha-helices (Fig. 4a), which we tentatively named LW modules. Superimposition of g164 LW modules 2–9 revealed a good structural overlap (Fig. 4b), while LW module 1 appeared to be different. The superimposition of the HB1s from PSR2 and g164 LW modules showed a good overlap (Fig. 4c) and alignment of the primary sequences confirmed the conserved position of amino acids involved in maintaining the structure, with the exception of the PSR2 L2 position, which was replaced by a conserved Trp in g164 (Fig. 4d). The presence of a SP and structural homology to the LWY domain, a fold found only in oomycete effectors, strongly support the hypothesis that the candidate genes found in the avrRpv3.1 locus encode putative effector proteins.

Candidate avrRpv3.1 proteins induce cell death in plants carrying Rpv3.1

Virulence toward Rpv3.1 was associated with the deletion of g164 and g165 (Fig. 3), making them the most promising candidates to be the cognate Rpv3.1 avirulence gene. Our objective is now to validate their capacity to trigger cell death in Rpv3.1-resistant cultivars, thereby confirming their recognition by the host.

We confirmed the presence of three genes in the avirulent strain INRA-Pv221 with a PCR on genomic DNA and the absence of the gene g164 and g165 in the virulent strain Pv412 (Fig. S20). RNA-seq data at 24, 48 and 72 h post-inoculation (hpi) revealed that g164, g165 and g166 are transcribed (Fig. S21A; doi: 10.57745/U6JECD). The results were confirmed with a semi-quantitative reverse transcription polymerase chain reaction revealing that all three genes are expressed in germinated spores and during infection (Fig. S21B). The expression pattern suggests weak constitutive expression.
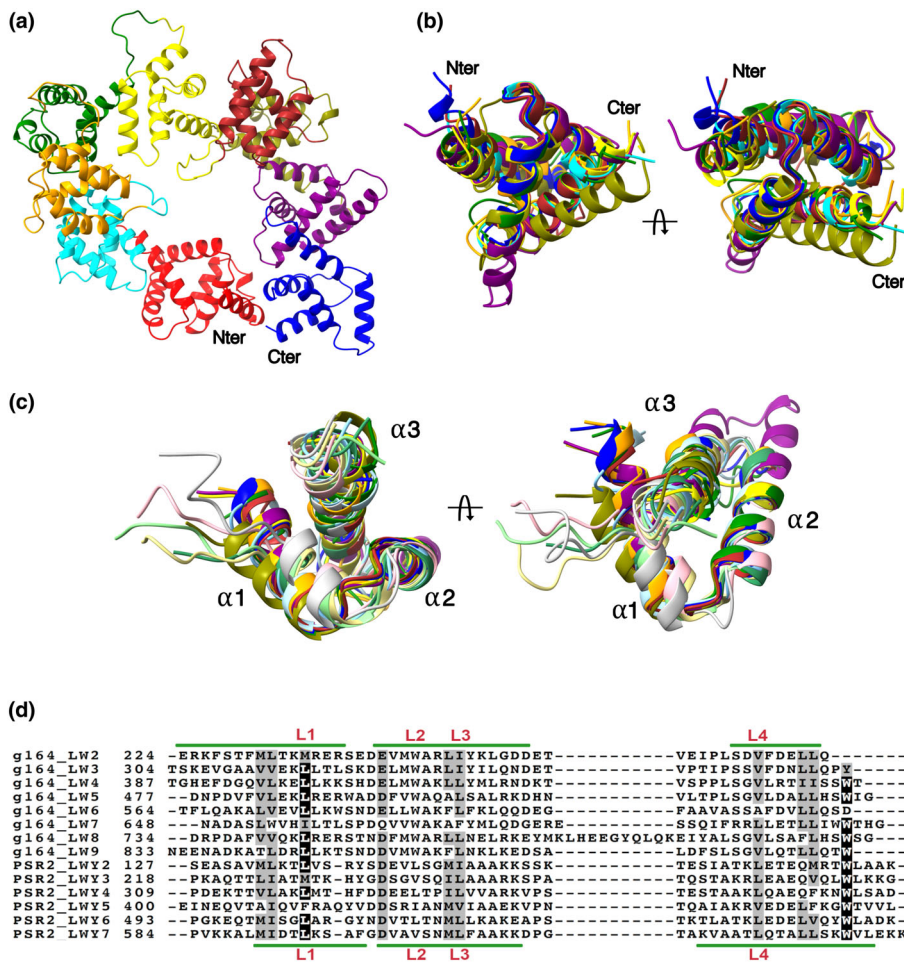
Fig. 4 Predicted tertiary structure of g164 is composed by modules containing the HB1 fold from the LWY domain. (a) Predicted structure of g164. The first 81 amino acids have been removed for clarity. Modules 1–9 are shown with different coloring (1–9: red, light blue, orange, green, yellow, brown, olive, purple, blue). The N terminus and C terminus of the molecule are represented by 'Nter' and 'Cter', respectively. (b) Superimposition of LW modules 2–9 from g164, seen from two different angles (curved arrow). Coloring as in A. The N- and C-terminal parts of the modules have been trimmed for clarity. (c) Superimposition of the N-terminal helix bundle 1 (HB1) from LWY-domains 2–7 from *Phytophthora sojae* PSR2 and the C-terminal HB1 from LW modules 2–9 of g164, seen from two different angles (curved arrow). Alpha-helices 1–3 are indicated. Coloring in g166 as in A. Coloring of PSR2 LWYs (2–7): light sky blue, khaki, sea green, silver, light pink and light green. (d) Alignment of the HB1 primary sequences from the g164 LW modules and the PSR2 LWYs. Green lines indicate alpha-helices 1–3 (from left to right) for g164_LW2 (top) and PSR2_LWY7 (bottom). Conserved Leu residues contribution to the HB1 fold are shown in red. Note that the conservation of a Trp in the g164_LWs at the L2 position. Black background shows identity and gray background shows similarity (75% cutoff).

We then assessed the Rpv3.1-dependent cell death-inducing activity of the proteins coded by g164, g165, and the closely related effector g166 by transient expression in grapevine leaves. We cloned the coding sequences for g164, g165 and g166, without the SP, from the reference avirulent *P. viticola* strain INRA-Pv221. Two alleles were obtained for g166, which we named g166p and g166h according to the original haplotype. The transient expression assays (Fig. 5) demonstrated that all genes induced cell death in Regent but not in the susceptible variety Syrah, lacking Rpv3.1 (Fig. S22). Notably, g166h exhibited a more consistent induction of cell death across the six experiments conducted (Figs 5, S22–S25). These findings strongly suggest that effector proteins from the avrRpv3.1 locus can effectively induce Rpv3.1-dependent cell death.

Discussion

By employing a GWAS approach, entailing the phenotyping of *P. viticola* strains and their whole-genome sequencing, we successfully identified the avrRpv3.1 locus involved in the interaction with the Rpv3.1-mediated resistance in grapevine. We presented compelling evidence, based on population genetics indices, that this locus displayed non-neutral characteristics and

demonstrated signs of positive selection on resistant hosts. Within this locus, the deletion of two coding genes (g164 and g165) is associated with the Rpv3.1 resistance breakdown. These two genes are part of a cluster of 11 closely related proteins, all exhibiting the characteristic traits of potential oomycete effectors, including the presence of a signal peptide and EER motif, structural similarities to known RXLR effectors and expression upon infection. Notably, these effector proteins possess an unusually large size for oomycetes, measuring *c.* 880 amino acids. To put this into perspective, the largest known oomycete effectors to date are PsPSR2 (670 aa; He *et al.*, 2019) and AVRcap1b (673 aa; Derevnina *et al.*, 2021), and an analysis of the RXLR effector repertoire across seven oomycete species encompassing 2126 proteins revealed only eight proteins exceeding 800 aa in size (He *et al.*, 2019). Through predicted structural modeling, we identified a modular arrangement within the candidate effector proteins, featuring repeats reminiscent of the LWY fold (He *et al.*, 2019). The structural similarity to the LWY domain, which is specific to oomycete effectors, strongly suggests that these proteins are *bona fide* effectors. Based on the predicted structure, the identified modules overlapped with the LWY fold only at the level of the HB1, suggesting a possible new fold in the effector repertoire of oomycetes. Before this research, no avirulence
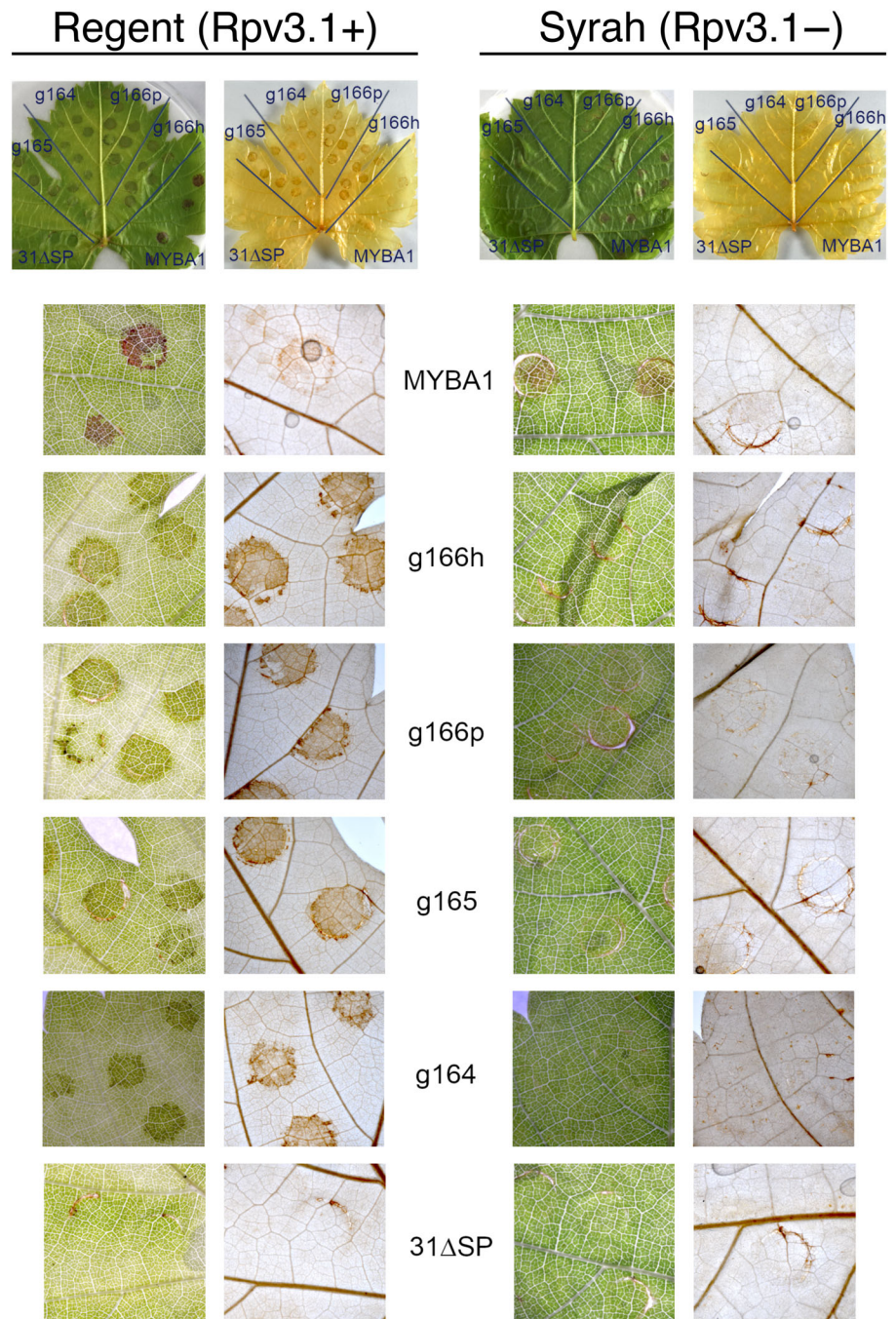
Fig. 5 Candidate effector proteins from the avrRpv3.1 locus induce cell death in plants carrying Rpv3.1. Cell death induction in leaves from the grapevine varieties Regent (Rpv3.1+) and Syrah (Rpv3.1−) 6 d after Agrobacterium-mediated expression of effector candidate genes g166h, g166p, g165 and g164. Agrobacterium-mediated expression of 31ΔSP, a *Plasmopara viticola* effector reported as not inducing cell death in grapevine (Combier *et al.*, 2019), was used as negative control for unspecific induction of cell death following agroinfiltration. Agrobacterium-mediated expression of VvMYBA, leading to the production of anthocyanins, was used as positive control to assess the efficiency of transformation. Images where chlorophyll was removed by incubating the leaves in 70% ethanol at 50°C are shown for clarity. The experiment was repeated with the same results (Supporting Information Fig. S23). The results of four additional experiments performed using GUS as a negative controls are presented in Figs S24 and S25.

genes had been characterized in the oomycete pathogen *P. viticola*. This study therefore presents the first-ever documentation of avirulence genes responsible for the breakdown of resistance in grapevine.

The experimental results showed that both candidate effectors (g164 and g165) and the closely related gene (g166) induce cell death in the presence of Rpv3.1, suggesting that the gene/s in the Rpv3.1 locus recognize all three effectors. The Rpv3.1 locus has been previously mapped to an interval containing two TIR-NB-LRR (TNL) genes, and it has been proposed that both genes are essential for conferring resistance (Foria *et al.*, 2020). This raises the possibility that each TNL gene interacts with different effectors, potentially exhibiting varying degrees of recognition strength. Another aspect to consider is the introgression of Rpv3.1 in Regent, which involves a 15 Mb linkage drag encompassing a cluster of nucleotide binding and leucine-rich repeat (NLR) genes (Foria *et al.*, 2020). It remains plausible that some of the candidate effector genes are recognized by other genes within this cluster. Overall, these findings suggest that Rpv3.1-mediated resistance may be the result of cumulative responses from the plant upon recognition of multiple effectors by one or more resistance genes. It should be noted that although the g166

gene seems to be recognized by the resistant plant, the absence of this effector does not seem to be required for strains to overcome resistance. One hypothesis to explain this result is that recognition of g166 alone may not be sufficient to halt pathogen infection. The absence of strains lacking only g166, together with the impossibility to transform *P. viticola*, hinders further investigation of the role of g166 in the interaction. Consequently, the loss of some of these effectors by the pathogen could lead to the breakdown of resistance. We indeed observed that the deletion of genes g164 and g165 is significantly associated with a high sporulation area on Rpv3.1-resistant hosts by *P. viticola* strains. The deletion of avirulence genes serves as an effective evolutionary strategy employed by pathogens to evade recognition and overcome plant defenses. Similar mechanisms have been documented in various fungal plant pathogens, including *Leptosphaeria maculans* (Daverdin *et al.*, 2012), *Zymoseptoria tritici* (Hartmann *et al.*, 2018) and *Melampsora larici-populina* (Louet *et al.*, 2021). In these cases, the loss of effector genes enhances the virulence of pathogens in Brassica crops, wheat and poplar, respectively.

The presence of a multi-gene effector family accompanied by a high density of TEs suggests genomic instability in the region. The rapid evolution of avirulence genes often occurs in genomic regions characterized by high TE content, punctual mutations and structural variations (Möller & Stukenbrock, 2017; Zaccaron *et al.*, 2022). Previous studies have shown that TE insertions near avirulence factors can have a significant impact on the virulence of fungal plant pathogens (Fouché *et al.*, 2020; Singh *et al.*, 2021; Wang *et al.*, 2021). Consistent with this notion, various structural variations such as deletions, inversions and recombinations were detected at the avrRpv3.1 locus. Another aspect of the locus variability lies in the range of deletion sizes observed, ranging from 14 to 96 kbp. TEs are likely to play a significant role in this genome evolution, as their mobility can expand the gene space through DNA duplication, interruption or induction of effector gene deletion (Bourque *et al.*, 2018; Muszewska *et al.*, 2019; Zaccaron *et al.*, 2022).

This study illustrates how structural variations can give rise to various mutational events, including complete or partial gene deletions, that lead to virulence. All of these events collectively contribute to a significant increase in the overall probability of mutations leading to virulence (Daverdin *et al.*, 2012). These findings may impact strategies for deploying grapevine resistance genes. In Europe, the focus is on enhancing resistance through pyramiding, a strategy involving stacking multiple resistance factors. The effectiveness and relative ranking of key deployment strategies (mixture, mosaic and pyramiding) in evolutionary and epidemiological control depend significantly on understanding the mutation rate leading to pathogen resistance breakdown (see Rimbaud *et al.*, 2021) for a review and (Zaffaroni *et al.*, 2024) for an application to grapevine downy mildew). With a high mutation rate, as observed in the evolution at the avrRpv3.1 locus, pyramiding may not necessarily be the most sustainable approach for preserving the efficacy of grapevine resistance genes (Zaffaroni *et al.*, 2024). However, drawing a general law from our results on Rpv3.1 resistance would be presumptuous. The

adaptation of the pathogen to host resistance is a phenomenon influenced by numerous determinants, and it should be considered on a case-by-case basis. Factors such as the impact of effector mutation on the strain's fitness need to be evaluated in each specific scenario.

The genetic variability observed at the avrRpv3.1 locus in the *P. viticola* population provides interesting insights into the origin of avr alleles. Notably, we found that one avr allele, avr1, was highly predominant in virulent strains of the *P. viticola* population (80% of the population), including the vir3.1 strain collected in Switzerland (Wingerter *et al.*, 2021). The presence of the avr1 allele in both Bordeaux (France) and Switzerland suggests the possibility of recurrent mutation at the avrRpv3.1 locus leading to the emergence of virulent strains. Alternatively, it is possible that the avr1 allele already preexisted at low frequencies in European populations of *P. viticola*, that is before the recent deployment of modern varieties carrying Rpv3.1. It should be noted that until the 1950s, French-American hybrids were extensively cultivated in Europe at large scale. It is therefore plausible that the avr1 allele, selected during that period, has persisted at low frequencies in *P. viticola* populations. Further investigations involving a more extensive survey across Europe would enhance our understanding of allele diversity at the avrRpv3.1 locus and the prevalence of these alleles in *P. viticola* populations.

In conclusion, our GWAS results and functional experiments converge toward the identification of effectors involved in the interaction with the Rpv3.1 resistance locus. Further molecular studies, focusing on the co-expression of candidate avirulence genes from the pathogen and resistance genes from the plant, will enhance the robustness of our study's findings. Our study also confirms the effectiveness of GWAS in identifying genomic loci involved in both qualitative traits, as illustrated by the discovery of the mating type locus of grapevine downy mildew (Dussert *et al.*, 2020), and quantitative traits, as demonstrated by the description of the locus responsible for the breakdown of a partial resistance in this study. We have demonstrated that the identification of effectors, typically located in rapidly evolving genomic regions, would not have been possible without the utilization of diploid-aware genome assemblies. This holds especially true for highly heterozygous species, such as *P. viticola* (Dussert *et al.*, 2019). Looking ahead, the availability of highly accurate long reads, such as HiFi reads (Cheng *et al.*, 2021, 2022), will greatly enhance our ability to obtain diploid references at the chromosome level. By leveraging such advanced techniques, we can unravel complex genomic traits and deepen our understanding of gene-for-gene interaction. While our current knowledge of the molecular interactions between downy mildew and its host is still in its early stages, our research contributes to expanding this knowledge and opens avenues for further exploration of gene-for-gene interaction in this pathosystem. The recent discoveries regarding the breakdown of the partial resistances Rpv10 and Rpv12 in grapevine (Heyman *et al.*, 2021; Wingerter *et al.*, 2021; Paineau *et al.*, 2022) pave the way for future exploration of new effectors in *P. viticola* using similar approaches.

Competing interests

None declared.

Author contributions

MP, FF and FD designed the research; MP, AM, PM, IDM, CC, FF and FD performed research; MP, AM, PM, TD, CC, FL, DC and FD performed the analyses; MP, AM, PM, FF, DC and FD wrote the manuscript; all authors edited the manuscript.

ORCID

Dario Cantu https://orcid.org/0000-0002-4858-1508
Carole Couture https://orcid.org/0000-0002-4348-213X
François Delmotte https://orcid.org/0000-0002-7138-8239
Thomas Dumartinet https://orcid.org/0000-0001-8648-5237
Frédéric Fabre https://orcid.org/0000-0001-8271-7678
Fabrice Legeai https://orcid.org/0000-0002-6472-4839
Isabelle D. Mazet https://orcid.org/0009-0007-3897-2808
Pere Mestre https://orcid.org/0000-0003-4488-6563
Andrea Minio https://orcid.org/0000-0003-2643-9209
Manon Paineau https://orcid.org/0000-0001-6881-1203

Data availability

The Illumina DNA sequences of *P. viticola* strains were submitted to NCBI SRA with project no. PRJNA875296. PacBio SMRT reads produced for INRA-Pv221 genome assembly were released under the project no. PRJNA329579. RNA-seq data were released under the project no. PRJNA329579. All data produced in this study are available at doi: 10.57745/MXJ-WZS and 10.57745/U6JECD.

References

Anderson RG, Deb D, Fedkenheuer K, McDowell JM. 2015. Recent progress in RXLR effector research. *Molecular Plant–Microbe Interactions* **28**: 1063–1072.

Bellin D, Peressotti E, Merdinoglu D, Wiedemann-Merdinoglu S, Adam-Blondon A-F, Cipriani G, Morgante M, Testolin R, Di Gaspero G. 2009. Resistance to *Plasmopara viticola* in grapevine 'Bianca' is controlled by a major dominant gene causing localised necrosis at the infection site. *Theoretical and Applied Genetics* **120**: 163–176.

Blum M, Waldner M, Gisi U. 2010. A single point mutation in the novel PvCesA3 gene confers resistance to the carboxylic acid amide fungicide mandipropamid in *Plasmopara viticola*. *Fungal Genetics and Biology* **47**: 499–510.

Bourque G, Burns KH, Gehring M, Gorbunova V, Seluanov A, Hammell M, Imbeault M, Izsvák Z, Levin HL, Macfarlan TS *et al*. 2018. Ten things you should know about transposable elements. *Genome Biology* **19**: 199.

Brilli M, Asquini E, Moser M, Bianchedi PL, Perazzolli M, Si-Ammour A. 2018. A multi-omics study of the grapevine-downy mildew (*Plasmopara viticola*) pathosystem unveils a complex protein coding- and noncoding-based arms race during infection. *Scientific Reports* **8**: 757.

Casagrande K, Falginella L, Castellarin SD, Testolin R, Di Gaspero G. 2011. Defence responses in Rpv3-dependent resistance to grapevine downy mildew. *Planta* **234**: 1097–1109.

Chen W-J, Delmotte F, Cervera SR, Douence L, Greif C, Corio-Costet M-F. 2007. At least two origins of fungicide resistance in grapevine downy mildew populations. *Applied and Environmental Microbiology* **73**: 5162–5172.

Cheng H, Concepcion GT, Feng X, Zhang H, Li H. 2021. Haplotype-resolved *de novo* assembly using phased assembly graphs with hifiasm. *Nature Methods* **18**: 170–175.

Cheng H, Jarvis ED, Fedrigo O, Koepfli K-P, Urban L, Gemmell NJ, Li H. 2022. Haplotype-resolved assembly of diploid genomes without parental data. *Nature Biotechnology* **40**: 1332–1335.

Chin C-S, Peluso P, Sedlazeck FJ, Nattestad M, Concepcion GT, Clum A, Dunn C, O'Malley R, Figueroa-Balderas R, Morales-Cruz A *et al*. 2016. Phased diploid genome assembly with single-molecule real-time sequencing. *Nature Methods* **13**: 1050–1054.

Combier M, Evangelisti E, Piron M-C, Rengel D, Legrand L, Shenhav L, Bouchez O, Schornack S, Mestre P. 2019. A secreted WY-domain-containing protein present in European isolates of the oomycete *Plasmopara viticola* induces cell death in grapevine and tobacco species. *PLoS ONE* **14**: e0220184.

Daverdin G, Rouxel T, Gout L, Aubertot J-N, Fudal I, Meyer M, Parlange F, Carpezat J, Balesdent M-H. 2012. Genome structure and reproductive behaviour influence the evolutionary potential of a fungal phytopathogen. *PLoS Pathogens* **8**: e1003020.

Delmas CEL, Fabre F, Jolivet J, Mazet ID, Cervera SR, Delière L, Delmotte F. 2016. Adaptation of a plant pathogen to partial host resistance: selection for greater aggressiveness in grapevine downy mildew. *Evolutionary Applications* **9**: 709–725.

Delmotte F, Mestre P, Schneider C, Kassemeyer H-H, Kozma P, Richart-Cervera S, Rouxel M, Delière L. 2014. Rapid and multiregional adaptation to host partial resistance in a plant pathogenic oomycete: evidence from European populations of *Plasmopara viticola*, the causal agent of grapevine downy mildew. *Infection, Genetics and Evolution, Journal of Molecular Epidemiology and Evolutionary Genetics of Infectious Diseases* **27**: 500–508.

Derevnina L, Chin-Wo-Reyes S, Martin F, Wood K, Froenicke L, Spring O, Michelmore R. 2015. Genome sequence and architecture of the tobacco downy mildew pathogen *Peronospora tabacina*. *Molecular Plant–Microbe Interactions* **28**: 1198–1215.

Derevnina L, Contreras MP, Adachi H, Upson J, Cruces AV, Xie R, Sklenar J, Menke FLH, Mugford ST, MacLean D *et al*. 2021. Plant pathogens convergently evolved to counteract redundant nodes of an NLR immune receptor network. *PLoS Biology* **19**: e3001136.

Di Gaspero G, Cipriani G, Adam-Blondon A-F, Testolin R. 2007. Linkage maps of grapevine displaying the chromosomal locations of 420 microsatellite markers and 82 markers for R-gene candidates. *Theoretical and Applied Genetics* **114**: 1249–1263.

Di Gaspero G, Copetti D, Coleman C, Castellarin SD, Eibach R, Kozma P, Lacombe T, Gambetta G, Zvyagin A, Cindrić P et al. 2012. Selective sweep at the Rpv3 locus during grapevine breeding for downy mildew resistance. *Theoretical and Applied Genetics* **124**: 277–286.

Dussert Y, Gouzy J, Richart-Cervera S, Mazet ID, Delière L, Couture C, Legrand L, Piron M-C, Mestre P, Delmotte F. 2016. Draft genome sequence of *Plasmopara viticola*, the grapevine downy mildew pathogen. *Genome Announcements* **4**: e00987-16.

Dussert Y, Legrand L, Mazet ID, Couture C, Piron M-C, Serre R-F, Bouchez O, Mestre P, Toffolatti SL, Giraud T et al. 2020. Identification of the first oomycete mating-type locus sequence in the grapevine downy mildew pathogen, *Plasmopara viticola*. *Current Biology* **30**: 3897–3907.

Dussert Y, Mazet ID, Couture C, Gouzy J, Piron M-C, Kuchly C, Bouchez O, Rispe C, Mestre P, Delmotte F. 2019. A high-quality grapevine downy mildew genome assembly reveals rapidly evolving and lineage-specific putative host adaptation genes. *Genome Biology and Evolution* **11**: 954–969.

European Commission. 2018. *Commission Implementig Regulation (EU) 2018/1981 of 13 December 2018 Renewing the Approval of the Active Substances Copper Compounds, as Candidates for Substitution, in Accordance with Regulation (EC) No 1107/2009 of the European Parliament and of the Council Concerning the Placing of Plant Protection Products on the Market, and Amending the Annex to Commission Implementing Regulation (EU) No 540/2011.* [WWW document] URL https://eur-lex.europa.eu/eli/reg_impl/2018/1981/oj [accessed 30 May 2023].

Feechan A, Anderson C, Torregrosa L, Jermakow A, Mestre P, Wiedemann-Merdinoglu S, Merdinoglu D, Walker AR, Cadle-Davidson L, Reisch B et al. 2013. Genetic dissection of a TIR-NB-LRR locus from the wild North American grapevine species *Muscadinia rotundifolia* identifies paralogous genes conferring resistance to major fungal and oomycete pathogens in cultivated grapevine. *The Plant Journal* **76**: 661–674.

Fontaine MC, Austerlitz F, Giraud T, Labbé F, Papura D, Richard-Cervera S, Delmotte F. 2013. Genetic signature of a range expansion and leap-frog event after the recent invasion of Europe by the grapevine downy mildew pathogen *Plasmopara viticola*. *Molecular Ecology* **22**: 2771–2786.

Fontaine MC, Labbé F, Dussert Y, Delière L, Richart-Cervera S, Giraud T, Delmotte F. 2021. Europe as a bridgehead in the worldwide invasion history of grapevine downy mildew, *Plasmopara viticola*. *Current Biology* **31**: 2155–2166.

Foria S, Copetti D, Eisenmann B, Magris G, Vidotto M, Scalabrin S, Testolin R, Cipriani G, Wiedemann-Merdinoglu S, Bogs J et al. 2020. Gene duplication and transposition of mobile elements drive evolution of the Rpv3 resistance locus in grapevine. *The Plant Journal* **101**: 529–542.

Fouché S, Badet T, Oggenfuss U, Plissonneau C, Francisco CS, Croll D. 2020. Stress-driven transposable element de-repression dynamics and virulence evolution in a fungal pathogen. *Molecular Biology and Evolution* **37**: 221–239.

Gao Y, Liu Z, Faris JD, Richards J, Brueggeman RS, Li X, Oliver RP, McDonald BA, Friesen TL. 2016. Validation of genome-wide association studies as a tool to identify virulence factors in *Parastagonospora nodorum*. *Phytopathology* **106**: 1177–1185.

Gessler C, Pertot I, Perazzolli M. 2011. *Plasmopara viticola*: a review of knowledge on downy mildew of grapevine and effective disease management. *Phytopathologia Mediterranea* **50**: 3–44.

Goddard TD, Huang CC, Meng EC, Pettersen EF, Couch GS, Morris JH, Ferrin TE. 2018. UCSF ChimeraX: meeting modern challenges in visualization and analysis. *Protein Science* **27**: 14–25.

Gómez Zeledón J, Kaiser M, Spring O. 2017. Exploring host-pathogen combinations for compatible and incompatible reactions in grapevine downy mildew. *European Journal of Plant Pathology* **149**: 1–10.

Gouy M, Guindon S, Gascuel O. 2010. SEAVIEW v.4: a multiplatform graphical user interface for sequence alignment and phylogenetic tree building. *Molecular Biology and Evolution* **27**: 221–224.

Hartmann FE, McDonald BA, Croll D. 2018. Genome-wide evidence for divergent selection between populations of a major agricultural pathogen. *Molecular Ecology* **27**: 2725–2741.

He J, Ye W, Choi DS, Wu B, Zhai Y, Guo B, Duan S, Wang Y, Gan J, Ma W et al. 2019. Structural analysis of *Phytophthora* suppressor of RNA silencing 2 (PSR2) reveals a conserved modular fold contributing to virulence. *Proceedings of the National Academy of Sciences, USA* **116**: 8054–8059.

Heyman L, Höfle R, Kicherer A, Trapp O, Ait Barka E, Töpfer R, Höfte M. 2021. The durability of quantitative host resistance and variability in pathogen virulence in the interaction between european grapevine cultivars and *Plasmopara viticola*. *Frontiers in Agronomy* **3**: 39.

Jumper J, Evans R, Pritzel A, Green T, Figurnov M, Ronneberger O, Tunyasuvunakool K, Bates R, Žídek A, Potapenko A et al. 2021. Highly accurate protein structure prediction with ALPHAFOLD. *Nature* **596**: 583–589.

Kariyawasam GK, Richards JK, Wyatt NA, Running KLD, Xu SS, Liu Z, Borowicz P, Faris JD, Friesen TL. 2022. The *Parastagonospora nodorum* necrotrophic effector SnTox5 targets the wheat gene Snn5 and facilitates entry into the leaf mesophyll. *New Phytologist* **233**: 409–426.

Kelley LA, Mezulis S, Yates CM, Wass MN, Sternberg MJE. 2015. The Phyre2 web portal for protein modeling, prediction and analysis. *Nature Protocols* **10**: 845–858.

Kurtz S, Phillippy A, Delcher AL, Smoot M, Shumway M, Antonescu C, Salzberg SL. 2004. Versatile and open software for comparing large genomes. *Genome Biology* **5**: R12.

Lan X, Liu Y, Song S, Yin L, Xiang J, Qu J, Lu J. 2019. *Plasmopara viticola* effector PvRXLR131 suppresses plant immunity by targeting plant receptor-like kinase inhibitor BKI1. *Molecular Plant Pathology* **20**: 765–783.

Lei X, Lan X, Ye W, Liu Y, Song S, Lu J. 2019. *Plasmopara viticola* effector PvRXLR159 suppresses immune responses in *Nicotiana benthamiana*. *Plant Signaling & Behavior* **14**: 1682220.

Li H. 2013. Aligning sequence reads, clone sequences and assembly contigs with BWA-MEM. *arXiv.* 13033997 Q-Bio.

Li H, Handsaker B, Wysoker A, Fennell T, Ruan J, Homer N, Marth G, Abecasis G, Durbin R, 1000 Genome Project Data Processing Subgroup. 2009. The sequence alignment/Map format and SAMTOOLS. *Bioinformatics* **25**: 2078–2079.

Liu J, Chen S, Ma T, Gao Y, Song S, Ye W, Lu J. 2021. *Plasmopara viticola* effector PvRXLR53 suppresses innate immunity in *Nicotiana benthamiana*. *Plant Signaling & Behavior* **16**: 1846927.

Louet C, Saubin M, Andrieux A, Persoons A, Gorse M, Pétrowski J, Fabre B, De Mita S, Duplessis S, Frey P et al. 2021. A point mutation and large deletion at the candidate avirulence locus AvrMlp7 in the poplar rust fungus correlate with poplar RMlp7 resistance breakdown. *Molecular Ecology* **32**: 2472–2483.

Ma T, Chen S, Liu J, Fu P, Wu W, Song S, Gao Y, Ye W, Lu J. 2021. *Plasmopara viticola* effector PvRXLR111 stabilizes VvWRKY40 to promote virulence. *Molecular Plant Pathology* **22**: 231–242.

Marone Fassolo E, Lecchi B, Marcianò D, Maddalena G, Toffolatti SL. 2022. Pathogen adaptation to American (Rpv3-1) and Eurasian (Rpv29) grapevine loci conferring resistance to downy mildew. *Plants* **11**: 2619.

Massonnet M, Cochetel N, Minio A, Vondras AM, Lin J, Muyle A, Garcia JF, Zhou Y, Delledonne M, Riaz S et al. 2020. The genetic basis of sex determination in grapes. *Nature Communications* **11**: 2902.

Maul. 2021. *Vitis international variety catalogue.* [WWW document] URL www.vivc.de [accessed 23 July 2021].

McKenna A, Hanna M, Banks E, Sivachenko A, Cibulskis K, Kernytsky A, Garimella K, Altshuler D, Gabriel S, Daly M et al. 2010. The genome analysis toolkit: a MapReduce framework for analyzing next-generation DNA sequencing data. *Genome Research* **20**: 1297–1303.

Merdinoglu D, Schneider C, Prado E, Wiedemann-Merdinoglu S, Mestre P. 2018. Breeding for durable resistance to downy and powdery mildew in grapevine. *OENO one* **52**: 203–209.

Merdinoglu D, Wiedeman-Merdinoglu S, Coste P, Dumas V, Haetty S, Butterlin G, Greif C. 2003. Genetic analysis of downy mildew resistance derived from *Muscadinia rotundifolia*. *Acta Horticulturae* **603**: 451–456.

Mestre P, Arista G, Piron M-C, Rustenholz C, Ritzenthaler C, Merdinoglu D, Chich J-F. 2017. Identification of a *Vitis vinifera* endo-β-1,3-glucanase with antimicrobial activity against *Plasmopara viticola*. *Molecular Plant Pathology* **18**: 708–719.

Mestre P, Carrere S, Gouzy J, Piron M-C, de Labrouhe DT, Vincourt P, Delmotte F, Godiard L. 2016. Comparative analysis of expressed CRN and RXLR effectors from two *Plasmopara* species causing grapevine and sunflower downy mildew. *Plant Pathology* 65: 767–781.

Miller ME, Nazareno ES, Rottschaefer SM, Riddle J, Pereira DDS, Li F, Nguyen-Phuc H, Henningsen EC, Persoons A, Saunders DGO *et al.* 2020. Increased virulence of *Puccinia coronata* f. sp. *avenae* populations through allele frequency changes at multiple putative Avr loci. *PLoS Genetics* 16: e1009291.

Minio A, Massonnet M, Figueroa-Balderas R, Castro A, Cantu D. 2019. Diploid genome assembly of the wine grape carménère. *G3: Genes, Genomes, Genetics* 9: 1331–1337.

Mirdita M, Schütze K, Moriwaki Y, Heo L, Ovchinnikov S, Steinegger M. 2022. COLABFOLD: making protein folding accessible to all. *Nature Methods* 19: 679–682.

Möller EM, Bahnweg G, Sandermann H, Geiger HH. 1992. A simple and efficient protocol for isolation of high molecular weight DNA from filamentous fungi, fruit bodies, and infected plant tissues. *Nucleic Acids Research* 20: 6115–6116.

Möller M, Stukenbrock EH. 2017. Evolution and genome architecture in fungal plant pathogens. *Nature Reviews. Microbiology* 15: 756–771.

Moroldo M, Paillard S, Marconi R, Fabrice L, Canaguier A, Cruaud C, De Berardinis V, Guichard C, Brunaud V, Le Clainche I *et al.* 2008. A physical map of the heterozygous grapevine "Cabernet Sauvignon" allows mapping candidate genes for disease resistance. *BMC Plant Biology* 8: 66.

Muszewska A, Steczkiewicz K, Stepniewska-Dziubinska M, Ginalski K. 2019. Transposable elements contribute to fungal genes and impact fungal lifestyle. *Scientific Reports* 9: 4307.

Paineau M, Mazet ID, Wiedemann-Merdinoglu S, Fabre F, Delmotte F. 2022. The characterization of pathotypes in grapevine downy mildew provides insights into the breakdown of Rpv3, Rpv10, and Rpv12 factors in grapevines. *Phytopathology* 112: 2329–2340.

Peressotti E, Wiedemann-Merdinoglu S, Delmotte F, Bellin D, Di Gaspero G, Testolin R, Merdinoglu D, Mestre P. 2010. Breakdown of resistance to grapevine downy mildew upon limited deployment of a resistant variety. *BMC Plant Biology* 10: 147.

Persoons A, Maupetit A, Louet C, Andrieux A, Lipzen A, Barry KW, Na H, Adam C, Grigoriev IV, Segura V *et al.* 2022. Genomic signatures of a major adaptive event in the pathogenic fungus *Melampsora larici-populina*. *Genome Biology and Evolution* 14: evab279.

Phan HTT, Furuki E, Hunziker L, Rybak K, Tan K-C. 2021. GWAS analysis reveals distinct pathogenicity profiles of Australian *Parastagonospora nodorum* isolates and identification of marker-trait-associations to septoria nodorum blotch. *Scientific Reports* 11: 10085.

Rimbaud L, Fabre F, Papaïx J, Moury B, Lannou C, Barrett LG, Thrall PH. 2021. Models of plant resistance deployment. *Annual Review of Phytopathology* 59: 125–152.

Rouxel M, Mestre P, Baudoin A, Carisse O, Delière L, Ellis MA, Gadoury D, Lu J, Nita M, Richard-Cervera S *et al.* 2014. Geographic distribution of cryptic species of *Plasmopara viticola* causing downy mildew on wild and cultivated grape in eastern North America. *Phytopathology* 104: 692–701.

Rouxel M, Mestre P, Comont G, Lehman BL, Schilder A, Delmotte F. 2013. Phylogenetic and experimental evidence for host-specialized cryptic species in a biotrophic oomycete. *New Phytologist* 197: 251–263.

Schwander F, Eibach R, Fechter I, Hausmann L, Zyprian E, Töpfer R. 2012. Rpv10: a new locus from the Asian Vitis gene pool for pyramiding downy mildew resistance loci in grapevine. *Theoretical and Applied Genetics* 124: 163–176.

Sharma R, Xia X, Cano LM, Evangelisti E, Kemen E, Judelson H, Oome S, Sambles C, van den Hoogen DJ, Kitner M *et al.* 2015. Genome analyses of the sunflower pathogen *Plasmopara halstedii* provide insights into effector evolution in downy mildews and *Phytophthora*. *BMC Genomics* 16: 741.

Shin J-H, Blay S, McNeney B, Graham J. 2006. LDHEATMAP: an R function for graphical display of pairwise linkage disequilibria between single nucleotide polymorphisms. *Journal of Statistical Software* 16: 1–9.

Siddique MI, Lee H-Y, Ro N-Y, Han K, Venkatesh J, Solomon AM, Patil AS, Changkwian A, Kwon J-K, Kang B-C. 2019. Identifying candidate genes for *Phytophthora capsici* resistance in pepper (*Capsicum annuum*) via genotyping-by-sequencing-based QTL mapping and genome-wide association study. *Scientific Reports* 9: 1–15.

Singh NK, Badet T, Abraham L, Croll D. 2021. Rapid sequence evolution driven by transposable elements at a virulence locus in a fungal wheat pathogen. *BMC Genomics* 22: 393.

Talevich E, Shain AH, Botton T, Bastian BC. 2016. CNVKIT: genome-wide copy number detection and visualization from targeted DNA sequencing. *PLoS Computational Biology* 12: e1004873.

Teufel F, Almagro Armenteros JJ, Johansen AR, Gíslason MH, Pihl SI, Tsirigos KD, Winther O, Brunak S, von Heijne G, Nielsen H. 2022. SIGNALP 6.0 predicts all five types of signal peptides using protein language models. *Nature Biotechnology* 40: 1023–1025.

Turner SD. 2018. QQMAN: an R package for visualizing GWAS results using Q-Q and manhattan plots. *Journal of Open Source Software* 3: 731.

Venuti S, Copetti D, Foria S, Falginella L, Hoffmann S, Bellin D, Cindrić P, Kozma P, Scalabrin S, Morgante M *et al.* 2013. Historical introgression of the downy mildew resistance gene Rpv12 from the Asian species *Vitis amurensis* into grapevine varieties. *PLoS ONE* 8: e61228.

Viennot-Bourgin G. 1949. *Les champignons parasites des plantes cultivees. Tome 2.* Paris, France: Masson.

Wang C, Milgate AW, Solomon PS, McDonald MC. 2021. The identification of a transposon affecting the asexual reproduction of the wheat pathogen *Zymoseptoria tritici*. *Molecular Plant Pathology* 22: 800–816.

Welter LJ, Göktürk-Baydar N, Akkurt M, Maul E, Eibach R, Töpfer R, Zyprian EM. 2007. Genetic mapping and localization of quantitative trait loci affecting fungal disease resistance and leaf morphology in grapevine (*Vitis vinifera* L.). *Molecular Breeding* 20: 359–374.

Wingerter C, Eisenmann B, Weber P, Dry I, Bogs J. 2021. Grapevine Rpv3-, Rpv10- and Rpv12-mediated defense responses against *Plasmopara viticola* and the impact of their deployment on fungicide use in viticulture. *BMC Plant Biology* 21: 470.

Wood KJ, Nur M, Gil J, Fletcher K, Lakeman K, Gann D, Gothberg A, Khuu T, Kopetzky J, Naqvi S *et al.* 2020. Effector prediction and characterization in the oomycete pathogen *Bremia lactucae* reveal host-recognized WY domain proteins that lack the canonical RXLR motif. *PLoS Pathogens* 16: e1009012.

Zaccaron AZ, Chen L-H, Samaras A, Stergiopoulos I. 2022. A chromosome-scale genome assembly of the tomato pathogen *Cladosporium fulvum* reveals a compartmentalized genome architecture and the presence of a dispensable chromosome. *Microbial Genomics* 8: 819.

Zaffaroni M, Rimbaud L, Rey J-F, Papaïx J, Fabre F. 2024. Effects of pathogen reproduction system on the evolutionary and epidemiological control provided by deployment strategies for two major resistance genes in agricultural landscapes. *Evolutionary Applications* 17: e13627.

Zhong Z, Marcel TC, Hartmann FE, Ma X, Plissonneau C, Zala M, Ducasse A, Confais J, Compain J, Lapalu N *et al.* 2017. A small secreted protein in *Zymoseptoria tritici* is responsible for avirulence on wheat cultivars carrying the Stb6 resistance gene. *New Phytologist* 214: 619–631.

Zhou X, Stephens M. 2012. Genome-wide efficient mixed-model analysis for association studies. *Nature Genetics* 44: 821–824.

Supporting Information

Additional Supporting Information may be found online in the Supporting Information section at the end of the article.

Fig. S1 Linear correlation between the sporulation area on Cabernet sauvignon and Regent.

Fig. S2 Histogram of the sporulation area of each of the 123 strains on Cabernet sauvignon and Regent.

Fig. S3 Principal component analysis realized with a subset of 18 069 single nucleotide polymorphisms.

Fig. S4 Quantile–quantile plot associated with Fig. 1.

Fig. S5 Manhattan plot of scaffolds Plvit038 and Plvit053 where the significant loci are located.

Fig. S6 Alignment of the sequences of Plvit038 and Plvit053 against INRA-Pv221 reference genome.

Fig. S7 Alignment of the sequences of the Haplotig_000014F_004 against the Primary_000014F.

Fig. S8 Maximum likelihood phylogenetic tree of the 11 protein sequences of *Plasmopara viticola* identified as avrRpv3.1-like genes and three similar proteins found in the closely related species *Plasmopara hasltedii*.

Fig. S9 Patterns of coverage in the locus (1/2).

Fig. S10 Patterns of coverage in the locus (2/2).

Fig. S11 Representation of the seven alleles identified in the 123 *Plasmopara viticola* strains analyzed in this study.

Fig. S12 Genomic structure at the avrRpv3.1 locus for each *Plasmopara viticola* strains associated with their phenotype.

Fig. S13 Patterns of coverage in the locus avrRpv3.1 of the strain 'avrRpv12−/3-' from Wingerter *et al.* (2021).

Fig. S14 Patterns of coverage in the locus avrRpv3.1 of the strain Pv412_11 from Paineau *et al.* (2022).

Fig. S15 Distribution of Weir and Cockerham FST across the entire contig and the specific FST value computed for the avrRpv3.1 locus.

Fig. S16 Conserved amino-acid motifs in avrRpv3.1-like proteins.

Fig. S17 Predicted tertiary structure of g164, g165, g166 and the superimposition of the three of them.

Fig. S18 Confidence metrics of the g164 predicted tertiary structure.

Fig. S19 g164 structural domains do not fit the LWY domain fold.

Fig. S20 PCRs on genomic DNA from *Plasmopara viticola* strain Pv221 and the strain 'Pv412_11'.

Fig. S21 Candidate effector genes from the AvrRpv3.1 locus are expressed in germinated spores and infected tissues.

Fig. S22 Candidate effector proteins from the AvrRpv3.1 locus induce cell death in plants carrying Rpv3.

Fig. S23 Candidate effector proteins from the AvrRpv3.1 locus induce cell death in plants carrying Rpv3.

Fig. S24 Candidate effector proteins from the AvrRpv3.1 locus induce cell death in plants carrying Rpv3.1. (6 d post-agroinfiltration).

Fig. S25 Candidate effector proteins from the AvrRpv3.1 locus induce cell death in plants carrying Rpv3.1. (10 d post-agroinfiltration).

Methods S1 *Plasmopara viticola* propagation.

Methods S2 *Plasmopara viticola* inoculation.

Methods S3 DNA extraction.

Methods S4 Sequencing.

Methods S5 Variant calling.

Methods S6 Quality control.

Methods S7 Population structure.

Methods S8 Genome reassembly procedure and annotation.

Methods S9 Phylogenetic analyses of the avrRpv3.1-like gene sequences.

Methods S10 Population genetic analysis.

Methods S11 avrRpv3.1 locus analysis of the virulent strain avrRpv12-/3- and Pv412.

Methods S12 Gene expression analysis.

Methods S13 Infiltration experiment.

Table S1 Statistics of the INRA-Pv221 genome reassembly.

Please note: Wiley is not responsible for the content or functionality of any Supporting Information supplied by the authors. Any queries (other than missing material) should be directed to the *New Phytologist* Central Office.